

03

## Study of the surface of nanocomposite thermoelectrics based on bismuth and antimony chalcogenides by scanning tunneling spectroscopy and atomic force microscopy

© L.N. Lukyanova, I.V. Makarenko, A.Yu. Samunin, A.A. Shabaldin, O.A. Usov

Ioffe Institute,  
St. Petersburg, Russia  
E-mail: lidia.lukyanova@mail.ioffe.ru

Received July 31, 2024

Revised August 9, 2024

Accepted October 16, 2024

The surface morphology of nanocomposite solid solutions of  $\text{Bi}_{0.45}\text{Sb}_{1.55}\text{Te}_{2.985}$  with  $\text{SiO}_2$  microinclusions and nanostructured polycrystalline samples of  $\text{Bi}_{0.45}\text{Sb}_{1.55}\text{Te}_{2.985}$  obtained by hot pressing was studied by atomic force microscopy (AFM) in semicontact mode. Optimization of the number, size of grains and nanofragments on the surface morphology images correlates with the thermoelectric properties, while in a nanocomposite with smaller grain sizes and nanofragments, the thermoelectric efficiency increases compared to polycrystal. The surface states of the Dirac fermions have been studied using scanning tunneling spectroscopy (STS). It is shown that the energy of the Dirac point  $E_D$ , the surface concentration of fermions  $n_s$  and the energy of surface levels formed by defects in pressed materials decrease compared to single crystals.

**Keywords:** bismuth telluride, solid solutions, nanocomposite, surface morphology, scanning tunneling spectroscopy, defect levels.

DOI: 10.61011/PSS.2024.11.60084.209

### 1. Introduction

Studies of nanostructured polycrystals and nanocomposite thermoelectrics based on bismuth and antimony chalcogenides pertaining to 3D topological insulators (TI) [1,2] are relevant, since these materials have high thermoelectric efficiency in the range of temperatures near and above room temperature up to 450 K [3–6]. The possibility of increasing the thermoelectric efficiency in such thermoelectrics is associated with nanostructuring and the addition of a small number of neutral nanoscale particles that do not interact with the matrix material. When a nanostructured solid solution of  $\text{Bi}_{0.3}\text{Sb}_{1.7}\text{Te}_3$  was studied the dimensionless thermoelectric efficiency  $ZT$  increased to 1.33 at 373 K with the addition of 0.4 vol.% Si [5], while without adding SiC the thermoelectric efficiency  $ZT = 1.23$  at 423 K.

The increase of thermoelectric efficiency  $Z$  in such thermoelectrics is determined by an increase of the Seebeck coefficient  $S$  and a decrease of thermal conductivity  $\kappa$ . The increase of the Seebeck coefficient in TI nanocomposites based on bismuth and antimony chalcogenides is determined by the effect of energy filtering and is associated with the formation of a potential barrier between the matrix material and inclusions of metallic or nonmetallic particles [7–10]. The potential barrier acts as a filter for scattering low-energy electrons, while high-energy electrons can pass through the barrier increasing the Seebeck coefficient [11]. The decrease of total thermal conductivity due to a decrease of the thermal conductivity of the crystal lattice occurs due to the intense scattering of phonons at the interfaces between grains in polycrystals and additional scattering centers in

nanocomposites [7–9,12]. Optimization of the technology for producing the considered thermoelectrics determines the morphology of the surface, which affects the thermoelectric properties.

As a rule, the surface morphology of bismuth telluride-based thermoelectrics is studied using scanning electron microscopy (SEM) and scanning transmission electron microscopy (STEM) methods [7–9,11]. Semi-contact method of atomic force microscopy (AFM) was used to study the surface morphology of nanostructured polycrystals of nonstoichiometric composition  $p\text{-Bi}_{0.45}\text{Sb}_{1.55}\text{Te}_{2.985}$  and nanocomposites  $p\text{-Bi}_{0.45}\text{Sb}_{1.55}\text{Te}_{2.985}$  with  $\text{SiO}_2$  microinclusions obtained by hot pressing of nanopowders [13].

The properties of the surface states of Dirac fermions were studied by scanning tunneling spectroscopy (STS) [14–16]. No similar studies of STS spectra in pressed nanocomposites and nanostructured polycrystals based on bismuth and antimony chalcogenides have been found in the literature.

The parameters of surface states in polycrystals and nanocomposites were determined from the analysis of local differential tunneling conductance  $dI_1/dU$  proportional to the electron density of states [17]. The results obtained are compared with the thermoelectric properties previously studied on the same samples [13].

### 2. Study of surface morphology by atomic force microscopy

Nanostructured polycrystalline samples of  $p\text{-Bi}_{0.45}\text{Sb}_{1.55}\text{Te}_{2.985}$  solid solutions and nanocomposites

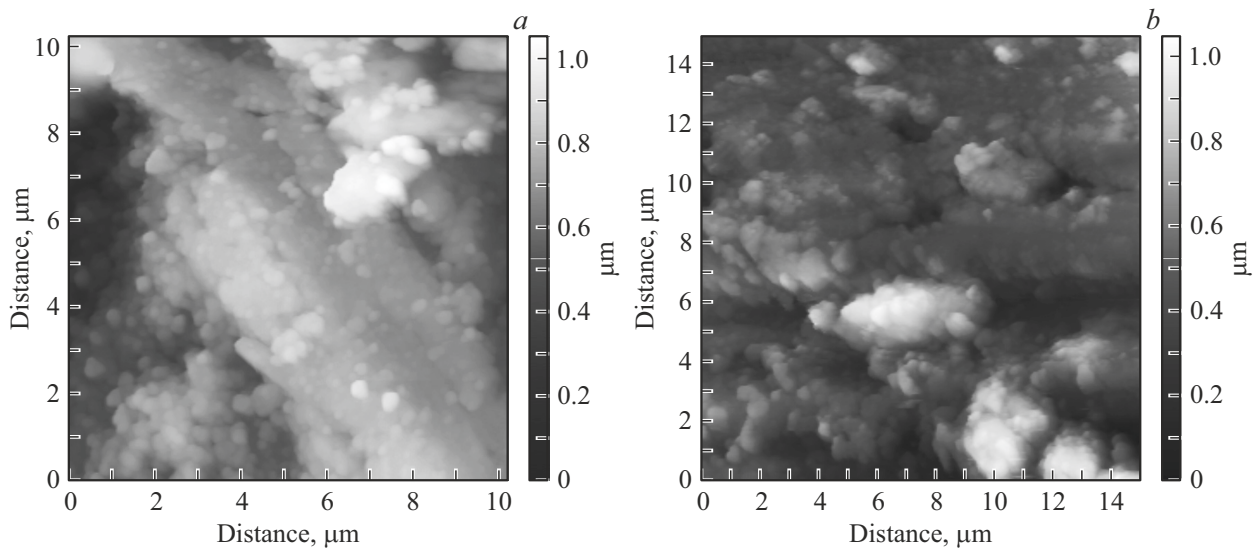


**Figure 1.** Morphology of the surface of  $p\text{-Bi}_{0.45}\text{Sb}_{1.55}\text{Te}_{2.985}$  solid solution: nanocomposites containing 3%  $\text{SiO}_2$  microinclusions (a) and nanostructured polycrystal (b) obtained by hot pressing.

containing 3 vol.%  $\text{SiO}_2$  microinclusions to study surface morphology by AFM and differential tunneling conductance spectra by STS method were obtained by hot pressing of nanopowders ground in a FRITSCH ball mill. The considered thermoelectrics pertain to layered Van der Waals crystals and consist of five-layer structures separated by Van der Waals slits along interlayer planes (0001) perpendicular to the crystallographic axis of the third order  $c_3$ . Nanopowders retain the layered crystal structure characteristic of bismuth and antimony chalcogenides [8]. The obtained micro- and nanoparticles are „flakes“, bounded by cleavage planes (0001) which were studied by AFM and STS methods. The thickness of the samples was about 3 mm.

Optimization of the processes of obtaining nanopowders and hot pressing parameters made it possible to obtain  $p\text{-Bi}_{0.45}\text{Sb}_{1.55}\text{Te}_{2.985}$  bulk nanocomposites with  $\text{SiO}_2$  microinclusions and  $p\text{-Bi}_{0.45}\text{Sb}_{1.55}\text{Te}_{2.985}$  nanostructured polycrystals with optimal thermoelectric properties near and below room temperature. According to the data from Ref. [13], the resulting nanocomposites had a lower concentration of carriers ( $p \approx 1.5 \cdot 10^{19} \text{ cm}^{-3}$ ) at the Seebeck coefficient  $S = 200 \mu\text{V} \cdot \text{K}^{-1}$ ) than nanostructured polycrystals ( $p = 4.5 \cdot 10^{19} \text{ cm}^{-3}$ ,  $S = 150 \mu\text{V} \cdot \text{K}^{-1}$ ) [13].

The average value of thermoelectric efficiency in the nanocomposite is  $\langle Z \rangle = 1.65 \cdot 10^{-3} \text{ K}^{-1}$  in the temperature range of 85–300 K and it is higher by 23%, and it is  $\langle Z \rangle = 2.5 \cdot 10^{-3} \text{ K}^{-1}$  in the range of 240–370 K and is higher by 12%, compared to the nanostructured polycrystal [13]. An increase of  $\langle Z \rangle$  to  $\langle Z \rangle = 1.7 \cdot 10^{-3} \text{ K}^{-1}$  is observed in the temperature range of 400–510 K in the nanostructured polycrystal, which is 10% higher than in the nanocomposite [13].

The increase of  $Z$  is associated with an increase of the Seebeck coefficient because of the effect of charge carrier

filtering by energies [7–10]. The lattice thermal conductivity decreased by an average of 25% due to an increase of the number of scattering centers in nanocomposites [13]. An increase of the Seebeck coefficient  $S$  and a decrease of lattice and total thermal conductivity is accompanied by an increase of the dependence of relaxation time on energy  $\tau(E)$ , which is typical for TI [11,18–20].

The surface morphology in  $p\text{-Bi}_{0.45}\text{Sb}_{1.55}\text{Te}_{2.985} + 3\% \text{SiO}_2$  nanocomposites and in  $p\text{-Bi}_{0.45}\text{Sb}_{1.55}\text{Te}_{2.985}$  polycrystalline samples was studied by the AFM method using device P47, CJSC „NT-MDT“, Zelenograd. Standard probes with a radius of curvature of the tip not exceeding 10 nm were used, and the maximum recorded height difference was up to  $2.5 \mu\text{m}$ . The statistical characteristics of the surface morphology were analyzed using nova1508 software (Figures 1–3).

The surface relief of  $p\text{-Bi}_{0.45}\text{Sb}_{1.55}\text{Te}_{2.985}$  thermoelectrics (Figure 1) consists of individual nanofragments, islands, terraces consisting of fused islands formed by diffusion processes and elastic stresses resulting from the surface deformation during hot pressing.

The average heights of nanofragments in various images of the surface of nanostructured polycrystals are  $0.59\text{--}0.74 \mu\text{m}$ , such heights in nanocomposites are  $0.37\text{--}0.75 \mu\text{m}$  (Figure 2). That is, the minimum heights of nanofragments in nanocomposites are lower than in polycrystals, while the maximum heights are close. It should be noted that the average heights of nanofragments on the interlayer surface (0001) are about 36 nm in single crystal samples of similar composition [21].

Histogram analysis showed (Figure 3) that the maximum number of nanofragments on the surface have heights within 330–395 nm in nanocomposites of  $\text{Bi}_{0.45}\text{Sb}_{1.55}\text{Te}_{2.985} + 3\% \text{SiO}_2$  solid solution and such heights increase in

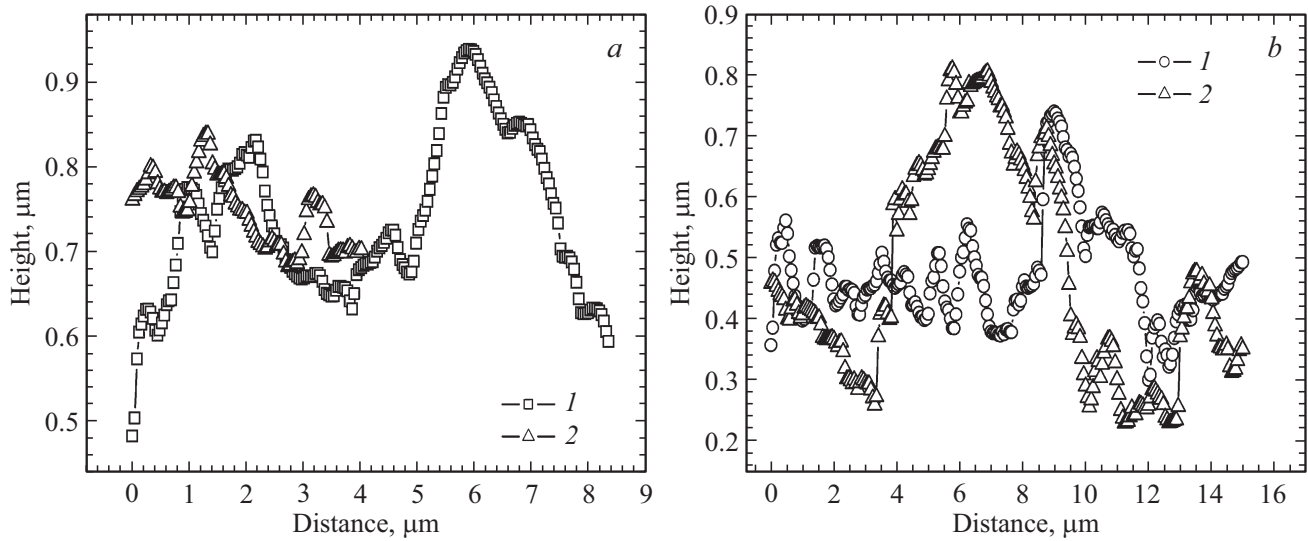


**Figure 2.** Characteristic profiles (1, 2) of the surface of samples of  $p\text{-Bi}_{0.45}\text{Sb}_{1.55}\text{Te}_{2.985}$  solid solution: nanocomposites containing 3%  $\text{SiO}_2$  microinclusions (a) and nanostructured polycrystal (b).

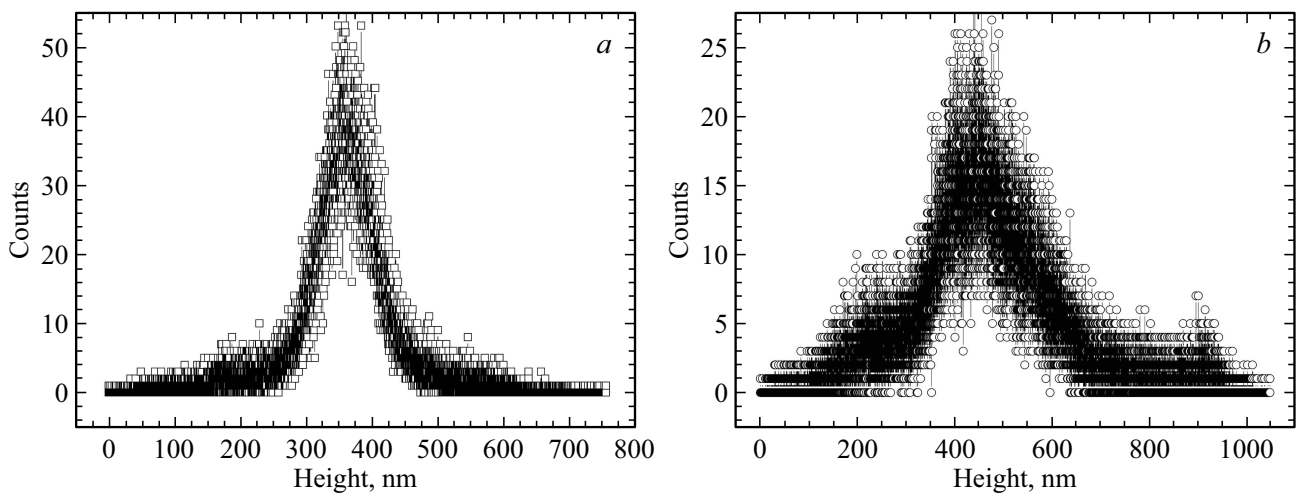


**Figure 3.** Distribution of the number of nanofragments depending on the height on the surface of  $p\text{-Bi}_{0.45}\text{Sb}_{1.55}\text{Te}_{2.985}$  solid solution: nanocomposites containing 3%  $\text{SiO}_2$  (a) microinclusions and nanostructured polycrystal (b).

polycrystals and range from 365 to 550 nm. The maximum heights of nanofragments reach 750 nm in nanocomposites and 1050 nm in polycrystals, and the minimum heights are 3 nm in both nanocomposites and polycrystals, while there are not more than three nanofragments with minimum and maximum heights.

Grains formed as a result of the fusion of individual nanofragments were found in the images of the surface of nanocomposite and polycrystalline samples. The largest number of grains have surface areas of 0.003–0.007 and 0.01–0.05  $\mu\text{m}^2$  in  $\text{Bi}_{0.45}\text{Sb}_{1.55}\text{Te}_{2.985}$  + 3%  $\text{SiO}_2$  nanocomposite. The number of such grains exceeds 90%.  $\text{SiO}_2$  microinclusions are represented in the nanocomposite in the form of grains with surface areas of up to 0.1  $\mu\text{m}^2$  with a content of 1.75 to 3%, which is

consistent with the composition of the nanocomposite. The number of small grains decreased to 20–30% in polycrystals, and grains with surface areas of 0.5–2.5  $\mu\text{m}^2$  account for about 60%.

Studies of the surface morphology of nanostructured polycrystals and nanocomposites have shown that the thermoelectric efficiency  $Z$  increases near room temperature and low temperatures in nanocomposites with smaller grain sizes than in polycrystals. The increase of efficiency  $Z$  in nanocomposites is attributable to a decrease of the thermal conductivity of the crystal lattice because of scattering on additional scattering centers formed by  $\text{SiO}_2$  microinclusions, and is accompanied by an increase of the Seebeck coefficient due to the effect of energy filtering of charge carriers [7–10].

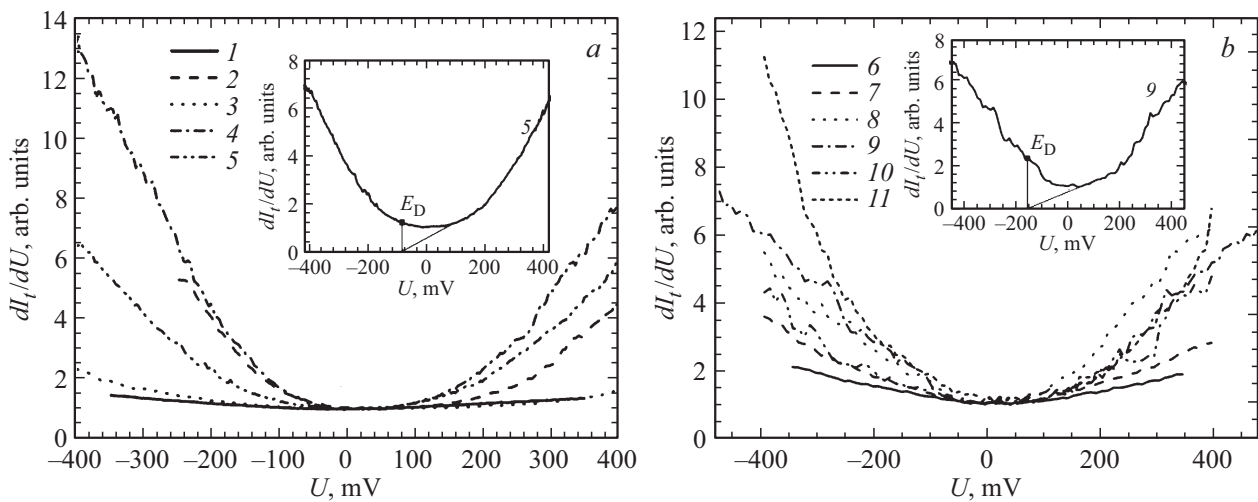


**Figure 4.** Normalized differential tunneling conductance  $dI_t/dU$  depending on voltage  $U$  in  $p\text{-Bi}_{0.45}\text{Sb}_{1.55}\text{Te}_{2.985}$  solid solution: nanocomposite containing 3%  $\text{SiO}_2$  microinclusions (a) and nanostructured polycrystal (b), measured on arbitrary surface fragments (1–5) and (6–11). The inserts show the position of the Dirac point  $E_D$  on the curve 5 and curve 9.

### 3. Differential tunneling conductance spectra

High-vacuum microscope GPI-300, combined with a high-vacuum measuring module was used to study local differential tunneling conductance spectra  $dI_t/dU$  by the STS method in  $p\text{-Bi}_{0.45}\text{Sb}_{1.55}\text{Te}_{2.985}+3\%$   $\text{SiO}_2$  nanocomposites and in  $p\text{-Bi}_{0.45}\text{Sb}_{1.55}\text{Te}_{2.985}$  polycrystalline samples. The possibility of studying the differential tunneling conductance spectra  $dI_t/dU$  by the STS method in  $p\text{-Bi}_{0.45}\text{Sb}_{1.55}\text{Te}_{2.985}$  pressed samples is attributable to the layered structure of thermoelectrics, which allows selecting fragments with cleavage planes (0001) located parallel to the plane of the sample holder. The dependencies  $dI_t/dU$  on the applied voltage  $U$  were used to determine the energy and fluctuations of the Dirac point  $E_D$  determined relative to the Fermi level  $E_F = 0$  (Figure 4).

The edge of the valence band is significantly distorted in  $p$ -type thermoelectrics based on bismuth and antimony chalcogenides greater than the edge of the conduction band in case of inversion of the band edges. Therefore, the position of the Dirac point  $E_D$  (Figure 4, inserts) in the considered thermoelectrics of the  $p$ -type of conductivity is determined by extrapolating the linear section of the dependence  $dI_t/dU$  to the abscissa axis [14,22], unlike thermoelectrics of the  $n$ -type, in which the position of  $E_D$  is determined by the minimum of  $dI_t/dU$ .

The analysis of the spectra measured on various parts of the sample surface showed that the energy  $E_D$  in nanocomposites containing  $\text{SiO}_2$  microparticles has a modulus less than that in polycrystalline samples. The average values of  $E_D$  are  $\langle E_D \rangle = -74$  meV in the studied nanocomposites, and  $\langle E_D \rangle = -126$  meV in polycrystalline samples, however, the fluctuations of the Dirac point have similar values and reach 18%.

Valence band edge energies  $E_v$  and conduction band edge energies  $E_c$  in  $dI_t/dU$  spectra of the studied thermoelectrics were determined from the normalized differential conductivity at the inflection points of the curve  $(dI_t/dU)/(I_t/U)$  as functions  $U$  (Figure 5) according to Refs. [17,23,24]. This special point was excluded with  $I_t = 0$ ,  $U = 0$  the function  $|I_t(U)| = 0$  because large distortions occur in its vicinity, which reduces the accuracy of determination of  $E_v$  and  $E_c$ . The Dirac point  $E_D$  is located in the band gap for all studied surface fragments of nanocomposite and polycrystalline samples (Figure 5), which is consistent with studies by angular resolution photoemission spectroscopy (ARPES) [25] and STS spectra [15] in films of similar composition.

The average energies  $\langle E_v \rangle$  and  $\langle E_c \rangle$  were  $-124$  and  $96$  meV for the nanocomposite, and values of  $-172$  and  $110$  meV were obtained for the nanostructured polycrystal. Fluctuations of the edge of the valence band  $E_v$  on various fragments of the surface of the nanocomposite and nanostructured polycrystal were similar and amounted to about 11%. Fluctuations of the edge of the conduction band  $E_c$  in the nanostructured polycrystal were weak (4%) and increased to 25% in the nanocomposite.

The average energy of the Dirac point  $\langle E_D \rangle = 50$  meV and the average energy of the Fermi level  $\langle E_F \rangle = 124$  meV in the nanocomposite when measured relative to the edge of the valence band  $E_v$ . Fluctuations  $\langle E_D \rangle$  were about 12% and fluctuations  $\langle E_F \rangle$  were 20%.  $\langle E_D \rangle = 45$  and  $\langle E_F \rangle = 172$  meV in a nanostructured polycrystal with fluctuations of 15% and 11%, respectively. It should be noted that the average energy of the Dirac point  $\langle E_D \rangle$  relative to  $E_v$  in compressed samples was lower than in thin epitaxial films according to ARPES data [25,15].

The width of the band gap  $E_g$  in the nanostructured polycrystalline sample is higher than in the nanocomposite in

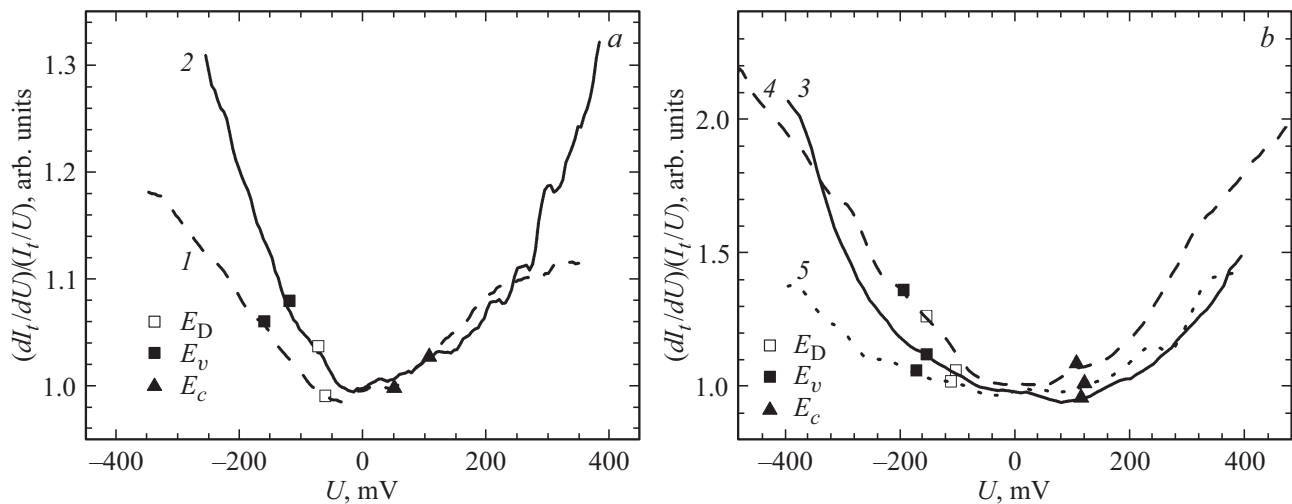


**Figure 5.** Ratios  $(dI_t/dU)/(I_t/U)$  depending on voltage  $U$  in  $p\text{-Bi}_{0.45}\text{Sb}_{1.55}\text{Te}_{2.985}$  solid solution: nanocomposite containing 3%  $\text{SiO}_2$  microinclusions of (a) and nanostructured polycrystal (b), as well as the position of the Dirac point  $E_D$ , the edges of the valence band  $E_v$  and conduction bands  $E_c$ .

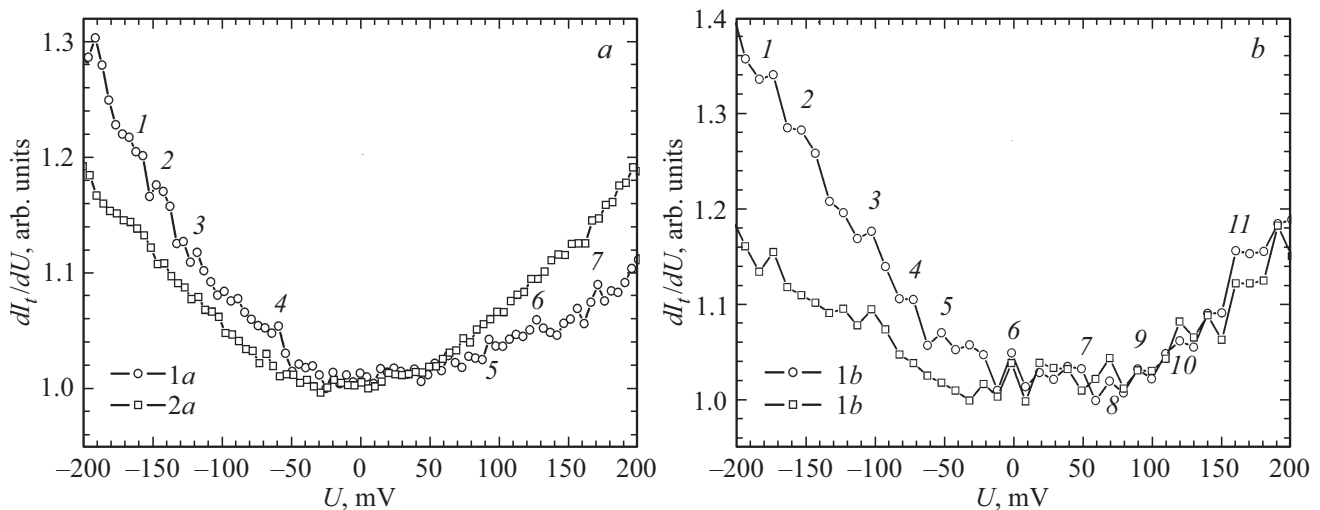


**Figure 6.** Positions of peaks at energies  $E_{pi}$  on the dependences of normalized differential tunneling conductance  $dI_t/dU$  on voltage  $U$  corresponding to surface defect levels for various fragments of  $p\text{-Bi}_{0.45}\text{Sb}_{1.55}\text{Te}_{2.985}$  solid solution: nanocomposite containing 3%  $\text{SiO}_2$  microinclusions (a, 1–7) and nanostructured polycrystals (b, 1–13).

accordance with the position of the band edges  $E_v$  and  $E_c$ , the average values  $\langle E_g \rangle$  are equal to 282 and 220 meV (Figure 5). Fluctuations of energy  $\langle E_g \rangle$  in the polycrystalline sample reached 20%, while fluctuations  $\langle E_g \rangle$  were weak in the nanocomposite and amounted to about 3%. An increase of  $E_g$  in pressed nanostructured polycrystals compared with a single crystal of similar composition, in which  $E_g = 237$  meV [25,26], leads to a shift of the onset of intrinsic conductance to higher temperatures [13].

Normalized dependences  $dI_t/dU$  on  $U$  showed peaks at energies  $E_{pi}$  corresponding to surface levels formed by defects that occur when Sb atoms are replaced by Te atoms in solid solutions and  $\text{SiO}_2$  microparticles are introduced (Figure 6, a, b). The defect energy  $E_P$  is defined as

the difference  $E_{pi} - E_D$ , where  $E_{pi}$  is the position of the corresponding peak (Figure 6, a, b).

The characteristic energy distribution of defect levels in different areas of the studied samples showed that the energy  $E_{P\min} = -59$  meV with the minimum modulus, necessary for the formation of defect levels, is observed in  $p\text{-Bi}_{0.45}\text{Sb}_{1.55}\text{Te}_{2.985} + \text{SiO}_2$  nanocomposites.  $E_{P\min}$  increases in modulus to  $-109$  meV in polycrystalline samples, and the maximum energy levels in absolute terms were close for nanocomposites and polycrystalline samples and reached 270–285 meV (Figure 7).

The energy of the Dirac point  $E_D$  together with the data for the Fermi velocity [25] allows estimating the surface concentration of fermions  $n_s$ , which determines

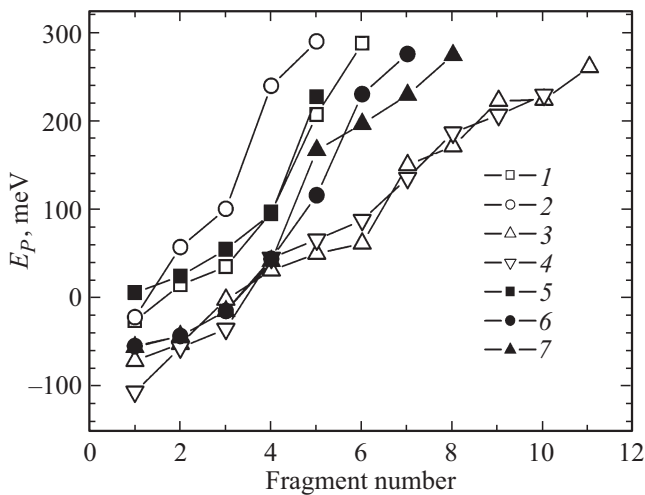


**Figure 7.** Distribution of defect level energy  $E_p$  on various fragments of  $p\text{-Bi}_{0.45}\text{Sb}_{1.55}\text{Te}_{2.985}$  nanostructured polycrystal (1–4) and  $p\text{-Bi}_{0.45}\text{Sb}_{1.55}\text{Te}_{2.985} + \text{SiO}_2$  nanocomposite (5–7).

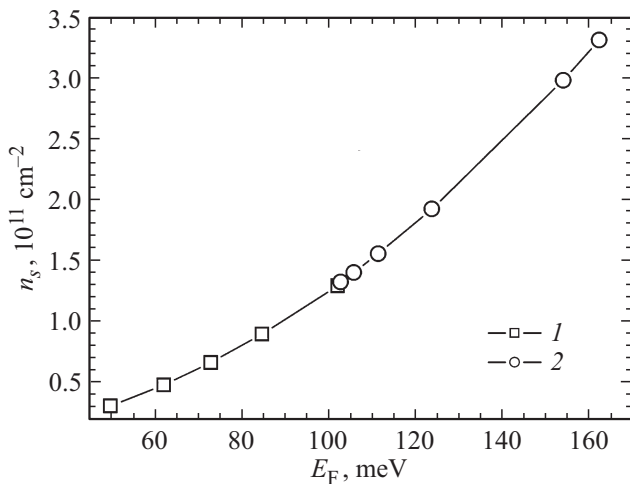


**Figure 8.** Surface concentration of Dirac fermions  $n_s$  depending on the Fermi energy  $E_F$  in  $p\text{-Bi}_{0.45}\text{Sb}_{1.55}\text{Te}_{2.985}$  solid solution: nanocomposites containing 3%  $\text{SiO}_2$  (1) microinclusions and nanostructured polycrystal (2).

the influence of the surface states of Dirac fermions on the properties of the material. Estimates of the surface concentration of fermions  $n_s$  indicate that the value  $n_s$ , calculated taking into account fluctuations of energy  $E_D$ , is higher in polycrystalline samples with optimal properties near and above room temperature. The surface concentration decreases at temperatures near and below room temperature in the studied nanocomposites with optimal properties (Figure 8). The value  $n_s$  increases with the increase of the Fermi energy  $E_F$ , which is determined relative to the Dirac point  $E_D$ , both in nanocomposites and nanostructured polycrystals (Figure 8).

An increase of the Seebeck coefficient  $S$  [13] and the effective mass of density of states  $m/m_0$  was observed in a

nanocomposite with a lower value  $n_s$  than in a polycrystal, as well as a decrease of the thermal conductivity of the crystal lattice  $\kappa_L$ . These values were calculated taking into account the change of the energy dependence of the relaxation time. The obtained ratios between  $n_s$ ,  $S$ ,  $m/m_0$  and  $\kappa_L$  determine the increase of thermoelectric efficiency  $Z$  in the nanocomposite, despite the increase of electrical conductivity in the polycrystal [13].

The surface concentration  $n_s$  was an order of magnitude higher in  $p\text{-Bi}_{0.5}\text{Sb}_{1.5}\text{Te}_3$  single crystal samples of similar composition with higher energy  $E_D$  [25,26] than in the pressed samples. The increase of electrical conductivity in single crystals [27,28] compared with nanocomposites was about 50%, while the values of the Seebeck coefficient were close. Thus, the contribution of surface states to thermoelectric properties in pressed polycrystals due to an increase of the surface concentration of fermions is higher than in nanocomposites, but lower than in single crystals, which are characterized by a higher surface concentration and Dirac point energy [25,26].

#### 4. Conclusion

It was found from the analysis of the morphology of the surface of nanostructured polycrystals and nanocomposites that the minimum heights of nanofragments and grains formed as a result of the fusion of nanofragments have smaller areas and heights in nanocomposites. There is a correlation between morphology and thermoelectric properties previously studied in similar pressed samples with the discovered ratio of surface morphology parameters in nanocomposites and nanostructured polycrystals. Nanocomposites with lower nanofragment heights and smaller grain areas showed an increase of thermoelectric efficiency  $Z$  compared to nanostructured polycrystals.

Studies of differential tunneling conductance spectra by the STS method in the considered materials for determining the characteristics of the surface electronic states of Dirac fermions have shown that the average energy of the Dirac point, the energy of defect levels, and the surface concentration of fermions, calculated taking into account fluctuations of the corresponding parameters, are lower in nanocomposites than in nanostructured polycrystals. It is found that the width of the band gap  $E_g$  in nanostructured polycrystals is higher than in nanocomposites, which results in a shift of the onset of intrinsic conductance to higher temperatures.

Estimates of the fermion surface concentration  $n_s$  have shown that the value  $n_s$ , calculated taking into account fluctuations of the energy of the Dirac point  $E_D$ , increases with the increase of  $E_D$  in both nanocomposites and polycrystals while  $n_s$  is higher in nanostructured polycrystals, which indicates an increase of the influence of surface states compared to nanocomposites. A comparison of pressed thermoelectrics with single crystals of similar composition indicates an increase of the influence of surface states on

the thermoelectric properties in single crystals due to an increase of the fermion surface concentration and Dirac point energy.

### Conflict of interest

The authors declare that they have no conflict of interest.

### References

- [1] M.J. Gilbert. *Commun. Phys.* **4**, *1*, 70 (2021).
- [2] J.P. Heremans, R.J. Cava, N. Samarth. *Nat. Rev. Mater.*, **2**, *10*, 17049 (2017).
- [3] B. Poudel, Q. Hao, Y. Ma, Y. Lan, A. Minnich, B. Yu, X. Yan, D. Wang, A. Muto, D. Vashaee, *Science* **320**, *2*, 634 (2008).
- [4] A.J. Minnich, M.S. Dresselhaus, Z.F. Ren, G. Chen. *Energy Environ. Sci.* **2**, *5*, 466 (2009).
- [5] J. Li, Q. Tan, J.-F. Li, D.-W. Liu, F. Li, Z.-Y. Li, M. Zou, K. Wang. *Adv. Funct. Mater.* **23**, *35*, 4317 (2013).
- [6] W. Liu, Z. Ren, G. Chen. *Thermoelectric Nanomaterials*. Springer, Heidelberg (2013). P. 255.
- [7] T.H. Nguyen, J. Enju, T. Ono. *J. Electrochem. Soc.* **166**, *12*, D508 (2019).
- [8] J. Zheng, Y. Kodera, X. Xu, S. Shin, K.M. Chung, T. Imai, R.V. Ichnfeldt, J.E. Garay, R.J. Chen. *J. Appl. Phys.* **130**, *23*, 235106 (2021).
- [9] B. Xu, M.T. Agne, T. Feng, T.C. Chasapis, X. Ruan, Y. Zhou, H. Zheng, J.-H. Bahk, M.G. Kanatzidis, G.J. Snyder, Y. Wu. *Adv. Mater.* **29**, *10*, 1605140 (2017).
- [10] E. Lee, J. Ko, J. Y. Kim, W.S. Seo, S.M. Choi, K.H. Lee, W. Shim, W. Lee. *J. Mater. Chem. C* **4**, *6*, 1313 (2016).
- [11] S.Y. Matsushita, K. Ichimura, K.K. Huynh, K. Tanigaki. *Phys. Rev. Mater.* **5**, *1*, 014205 (2021).
- [12] J.R. Szczech, J.M. Higgins, S. Jin. *J. Mater. Chem.* **21**, *12*, 4037 (2011).
- [13] A.A. Shabal'din, P.P. Konstantinov, D.A. Kurdyukov, L.N. Lukyanova, A.Yu. Samunin, E.Yu. Stovpiaga, A.T. Burkov. *Semiconductors*, **53**, *6*, 742 (2019).
- [14] Z. Alpichshev, J.G. Analytis, J.-H. Chu, I.R. Fisher, Y.L. Chen, Z.X. Shen, A. Fang, A. Kapitulnik. *Phys. Rev. Lett.* **104**, *1*, 016401 (2010).
- [15] X. He, H. Li, L. Chen, K. Wu. *Sci. Rep.* **5**, *1*, 8830 (2015).
- [16] T. Hanaguri, K. Igarashi, M. Kawamura, H. Takagi, T. Sasa-gawa. *Phys. Rev. B* **82**, *8*, 081305(R) (2010).
- [17] H. Nam, Y. Xu, I. Miotkowski, J. Tian, Y.P. Chen, C. Liu, C.K. Shih. *J. Phys. Chem. Solids* **128**, 251 (2019).
- [18] K. Nomura, A.H. MacDonald. *Phys. Rev. Lett.* **98**, *7*, 076602 (2007).
- [19] K. Nomura, M. Koshino, S. Ryu. *Phys. Rev. Lett.* **99**, *14*, 146806 (2007).
- [20] L.N. Lukyanova, Y.A. Boikov, O.A. Usov, V.A. Danilov, I.V. Makarenko, V.N. Petrov. *Magnetochemistry* **9**, *6*, 141 (2023).
- [21] L.N. Lukyanova, A.Yu. Bibik, V.A. Aseev, O.A. Usov, I.V. Makarenko, V.N. Petrov, N.V. Nikonorov, V.A. Kutasov. *Phys. Solid State*, **58**, *7*, 1440 (2016).
- [22] M. Chen, J. Peng, H. Zhang, L. Wang, K. He, X. Ma, Q. Xue. *Appl. Phys. Lett.* **101**, *8*, 081603 (2012).
- [23] C. Wagner, R. Franke, T. Fritz. *Phys. Rev. B* **75**, *23*, 235432 (2007).
- [24] J.A. Stroschio, R.M. Feenstra. *A.P. Fein. Phys. Rev. Lett.* **57**, *20*, 2579 (1986).
- [25] J. Zhang, C.-Z. Chang, Z. Zhang, J. Wen, X. Feng, K. Li, M. Liu, K. He, L. Wang, X. Chen, Q.-K. Xue, X. Ma, Y. Wang. *Nat. Commun.* **2**, *1*, 574 (2011).
- [26] L.N. Lukyanova, I.V. Makarenko, O.A. Usov, P.A. Dementev. *Semicond. Sci. Technol.* **33**, *5*, 055001 (2018).
- [27] L.N. Lukyanova, A.A. Shabal'din, A.Yu. Samunin, O.A. Usov. *Semiconductors* **56**, *1*, 10 (2022).
- [28] L.N. Lukyanova, Yu.A. Boikov, O.A. Usov, V.A. Danilov. *Semiconductors* **51**, *6*, 692 (2017).

*Translated by A.Akhtyamov*